THE JOURNAL OF BIOLOGICAL CHEMISTRY VOL. 285, NO. 24, pp. 18433–18442, June 11, 2010

Quinol-cytochrome *c* Oxidoreductase and Cytochrome c_4 Mediate Electron Transfer during Selenate Respiration in *Thauera selenatis*[*] [S]

Received for publication, February 19, 2010, and in revised form, April 1, 2010 Published, JBC Papers in Press, April 13, 2010, DOI 10.1074/jbc.M110.115873

Elisabeth C. Lowe[‡1], Sarah Bydder[§2], Robert S. Hartshorne[¶], Hannah L. U. Tape[‡], Elizabeth J. Dridge[‡], Charles M. Debieux[‡], Konrad Paszkiewicz[‡], Ian Singleton[‖], Richard J. Lewis[**], Joanne M. Santini[‡‡], David J. Richardson[¶], and Clive S. Butler[‡3]

From the [‡]School of Biosciences, Centre for Biocatalysis, University of Exeter, Stocker Road, Exeter EX4 4QD, United Kingdom, the [§]Department of Microbiology, La Trobe University, 3086 Victoria, Australia, the [¶]School of Biological Sciences, University of East Anglia, Norwich NR4 7TJ, United Kingdom, the [‖]Institute for Research on Environment and Sustainability, University of Newcastle, Newcastle upon Tyne NE2 4HH, United Kingdom, the [**]Institute for Cell and Molecular Biosciences, University of Newcastle, Newcastle upon Tyne NE2 4HH, United Kingdom, and the [‡‡]Institute of Structural and Molecular Biology, University College London, Gower Street, London WC1E 6BT, United Kingdom

Selenate reductase (SER) from *Thauera selenatis* is a periplasmic enzyme that has been classified as a type II molybdoenzyme. The enzyme comprises three subunits SerABC, where SerC is an unusual *b*-heme cytochrome. In the present work the spectropotentiometric characterization of the SerC component and the identification of redox partners to SER are reported. The mid-point redox potential of the *b*-heme was determined by optical titration (E_m + 234 ± 10 mV). A profile of periplasmic *c*-type cytochromes expressed in *T. selenatis* under selenate respiring conditions was undertaken. Two *c*-type cytochromes were purified (~24 and ~6 kDa), and the 24-kDa protein (cyt*c*-Ts4) was shown to donate electrons to SerABC *in vitro*. Protein sequence of cyt*c*-Ts4 was obtained by N-terminal sequencing and liquid chromatography-tandem mass spectrometry analysis, and based upon sequence similarities, was assigned as a member of cytochrome c_4 family. Redox potentiometry, combined with UV-visible spectroscopy, showed that cyt*c*-Ts4 is a diheme cytochrome with a redox potential of +282 ± 10 mV, and both hemes are predicted to have His-Met ligation. To identify the membrane-bound electron donors to cyt*c*-Ts4, growth of *T. selenatis* in the presence of respiratory inhibitors was monitored. The specific quinol-cytochrome *c* oxidoreductase (QCR) inhibitors myxothiazol and antimycin A partially inhibited selenate respiration, demonstrating that some electron flux is via the QCR. Electron transfer via a QCR and a diheme cytochrome c_4 is a novel route for a member of the DMSO reductase family of molybdoenzymes.

Within the DMSO reductase family of type II molybdoenzymes (1) there is a distinct clade of enzymes that are translocated to the periplasm using the twin arginine translocation (TAT)[4] pathway (2, 3) and possess a monomeric *b*-type heme-containing γ-subunit (1). The enzymes within this clade function as either dehydrogenases (*e.g.* ethylbenzene dehydrogenase (EBDH) from *Aromatoleum aromaticum* (4) and dimethylsulfide dehydrogenase from *Rhodovulum sulfidophilum* (1, 5)) or reductases (*e.g.* selenate reductase from *Thauera selenatis* (6, 7) and chlorate reductase from *Ideonella dechloratans* (8, 9)) and catalyze either hydride or oxygen transfer as generalized by Reaction 1.

$$X + H_2O \leftrightarrows XO + 2H^+ + 2e^-$$

REACTION 1

These soluble enzymes consist of three subunits and in addition to the *b*-heme cytochrome (γ-subunit), they comprise an iron-sulfur protein (β-subunit) coordinating 1 × [3Fe-4S] cluster and 3 × [4Fe-4S] clusters, and a catalytic component (α-subunit) that coordinates a [4Fe-4S] cluster and the active site molybdopterin guanine dinucleotide cofactor (10, 11) (Fig. 1). The reductases play a pivotal function, coupling the reduction of substrates to the generation of the proton-motive force (PMF). Identifying the route by which electrons are transferred to these reductases is vital to understanding their bioenergetics (12). How periplasmic substrate reduction can generate a PMF, which is sufficient to support growth, is of considerable interest. The use of selenate and selenite as bacterial respiratory substrates has been well documented (13). By far the most well studied selenate-respiring bacterium has been *T. selenatis*; however, the characterization of the selenate respiratory sys-

* This work was funded in part by Biotechnology and Biological Sciences Research Council (BBSRC) Grants P17219 and BBS/B/10110 (to C. S. B. and D. J. R.) and BBSRC/Engineering and Physical Sciences Research Council (life science interface) Grant BB/D00781X/1 (to C. S. B., R. J. L., and D. J. R.). Sequencing of the *T. selenatis* genome was funded by the Systems Biology Theme, University of Exeter.

[S] The on-line version of this article (available at http://www.jbc.org) contains supplemental Figs. S1 and S2.

[1] A recipient of a BBSRC Agri-food committee studentship.

[2] Supported by a La Trobe University postgraduate award.

[3] To whom correspondence should be addressed: School of Biosciences, Centre for Biocatalysis, University of Exeter, Stocker Road, Exeter EX4 4QD, United Kingdom. Tel.: 44-1329-264-675; Fax: 44-1392-263-434; E-mail: c.s.butler@exeter.ac.uk.

[4] The abbreviations used are: TAT, twin-arginine translocation; SER, periplasmic selenate reductase; NAR, membrane-bound nitrate reductase; EBDH, ethylbenzene dehydrogenase; DMSDH, dimethylsulfide dehydrogenase; FDH, formate dehydrogenase; FeS/FS0, iron-sulfur clusters; HQNO, 2-*n*-heptyl-4-hydroxyquinoline *N*-oxide; QCR, quinol-cytochrome *c* oxidoreductase; QDH, quinol dehydrogenase; DH, primary dehydrogenase; PMF, proton-motive force; cytc-Ts1 through -Ts7, *T. selenatis* soluble *c*-type cytochromes 1 to 7; pNAR, NAR on positive side of membrane .

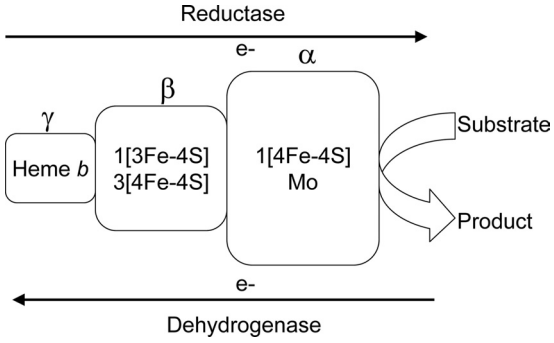

FIGURE 1. **Subunit organization and redox cofactors of periplasmic type II molybdoenzymes.** Direction of electron transfer is indicated by the *arrows*. Reductases include selenate and chlorate reductase. Dehydrogenases include dimethylsulfide and ethylbenzene dehydrogenases.

tem has not yet addressed the mechanism by which electrons are transferred from the cytoplasmic membrane to the periplasmic selenate reductase (SerABC). Because SerABC appears to be soluble and not associated with the inner or outer membrane (6), it is likely that another protein acts as a shuttle to take electrons from the membrane and deliver them to the *b*-heme of SerC. Reduced SerC then donates electrons, via the iron-sulfur clusters of SerAB (11), specifically to the molybdopterin cofactor for reduction of selenate (SeO_4^{2-}) to selenite (SeO_3^{2-}) (6, 11, 14).

The *b*-heme of SerC is presumed to be the site of electron entry to the selenate reductase (SER) enzyme complex but also remains poorly studied. The recently solved crystal structure of EBDH reveals that its γ-subunit also binds an unusual *b*-type heme, which is coordinated by methionine and lysine ligands (15). This coordination favors the uncharged ferrous heme over the charged ferric form and as such modulates a relatively high redox potential of +254 mV. Similarly, optical potentiometric redox titrations of the heme *b* in the γ-subunit of dimethylsulfide dehydrogenase (DMSDH) revealed a high redox potential of $E_m = +324$mV (10). By contrast, the cytoplasmic-facing respiratory nitrate reductase NAR from *Escherichia coli* (another member of the type II molybdoenzymes) possesses a membrane-bound γ-subunit (NarI) that coordinates two *bis*-His-ligated *b*-hemes that have much lower redox potentials at +20 and +120 mV (16). In the case of NAR, the low redox potentials of the heme favors electron flow away from NarI, toward the molybdenum guanine dinucleotide cofactor in NarG, and ultimately resulting in the reduction of nitrate to nitrite. Critically, the dehydrogenases (EBDH and DMSDH) function in the reverse direction (Fig. 1); it has been argued that, due to the unusually high potential *b*-heme in γ-subunits of both EBDH and DMSDH, that the γ-subunit is the site of electron egress from these enzymes to their redox partners (10, 15). Consequently, the high potential *b*-heme might function to draw electrons away from, rather than toward, the molybdopterin guanine dinucleotide cofactor during catalysis as displayed in the nitrate reductase enzymes. Analysis of the amino acid sequence alignment of EBDH and DMSDH with selenate reductase (SER) shows that the coordinating methionine (Met-138) and lysine (Lys-228) residues are also conserved in SerC. This then raises interesting questions as to what is the redox potential for the *b*-heme in the reductase members of this distinct type II clade and what are the likely redox partners?

Among the related type II molybdoenzymes, there are a number of different routes of electron transfer to terminal reductases, although the majority catalyze reactions with a lower redox potential than the selenate/selenite couple (+475 mV). For example; the DMSO/DMS couple is +160 mV and trimethylamine *N*-oxide/trimethylamine couple is +130 mV (17). Within the DMSO reductase group, a number of pathways for electron transport have been established, and a variety of membrane-bound proteins have been implicated. These membrane-bound cytochromes are responsible for extracting electrons from the quinol pool so that they can be transferred to the associated downstream terminal reductases. The existing literature provides several routes by which electrons are transferred. For example, the membrane-bound nitrate reductase NarGH (16, 18) receives its electrons from its dedicated NarI membrane integral subunit, which contains two *b*-hemes; the DMSO reductase from *E. coli* has a similar organization of subunits (17), but faces the periplasm. The *E. coli* trimethylamine *N*-oxide reductase TorA (*Rhodobacter* sp.), DMSO reductase DorA (17), and the periplasmic nitrate reductase NapAB (19) accept electrons from dedicated tetra- or penta-heme quinol dehydrogenases in the membrane (TorC/DorC/NapC). In the case of Nap, there is also an alternative pathway; the *nap* gene cluster in *E. coli* for example, also contains *napG* and *napH*, which encode iron-sulfur proteins responsible for electron transfer from ubiquinol to NapC (20).

It may be the case that selenate respiration in *T. selenatis* does not occur via any of these known pathways; McEwan *et al.* (21) postulated that the selenate reductase of *T. selenatis* could receive electrons from quinol-cytochrome *c* oxidoreductase (QCR) via a high potential *c*-type cytochrome, due to the high potential of the selenate/selenite couple. This has not been seen for any of the other type II molybdoenzymes, so showing electron donation from QCR, via a soluble cytochrome *c* to SerABC, would represent a novel electron transport chain within this group. The aim of the present work was to resolve the electron transfer pathways during selenate respiration in *T. selenatis*.

EXPERIMENTAL PROCEDURES

Growth of T. selenatis, Production of Periplasmic Fractions, and Purification of SER—T. selenatis was grown anaerobically at 30 °C in mineral salts medium (6) containing yeast extract (0.1%), with either selenate or nitrite (10 mM) as terminal electron acceptors and acetate (10 mM) as the electron donor in 10-liter batch cultures. Cultures were harvested during late log phase (after 16–18 h growth) at A_{600} 0.6–0.7, and spheroplasts were prepared as described previously (6). The spheroplasts were removed by centrifugation (25,000 × *g*, 20 min), and the supernatant, containing the periplasm, was retained. Periplasms were analyzed by SDS-PAGE, and *c*-type cytochromes were visualized using the heme stain method. SER was purified as detailed by Schröder *et al.* (6) with the modifications noted by Dridge *et al.* (11). Purified enzyme was stored at −80 °C. Purity was determined by SDS-PAGE, and positive identification of the presence of the SerC component was

achieved by N-terminal sequence analysis as described previously (22).

Purification of c-type Cytochromes—Soluble protein from a 10-liter culture was loaded onto a Q-Sepharose Fast-Flow anion-exchange column (70-ml bed volume, Amersham Biosciences) pre-equilibrated with 3 column volumes of 30 mM Tris, pH 8.5. The column was washed with a further column volume of buffer to remove unbound proteins. A 24-kDa *c*-type cytochrome was eluted using a 300-ml gradient of 0–300 mM NaCl in 30 mM Tris, pH 8.5. Protein concentration was monitored using absorbance at 280 nm, and the presence of cytochromes was monitored using absorbance at 410 nm. The fractions containing the 24-kDa *c*-type cytochrome as determined by SDS-PAGE were pooled and concentrated using a 15-ml 10-kDa molecular weight cut-off centrifugal concentrator at 4000 × *g*. The concentrated protein was loaded onto a Superdex 200 16/60 gel-filtration column (Amersham Biosciences) equilibrated with 2 column volumes of 30 mM Tris, pH 8.5, and eluted in the same buffer. The fractions containing the 24-kDa *c*-type cytochrome were pooled and loaded onto a 1-ml Mono Q anion-exchange column (Amersham Biosciences) equilibrated with 30 mM Tris, pH 8.5, and eluted with a gradient of 0–1 M NaCl in 30 mM Tris, pH 8.5. As a final purification step, the fractions containing the 24-kDa *c*-type cytochrome were pooled and transferred to dialysis tubing (6-kDa MWCO, Fisher), and the protein was then dialyzed overnight at 4 °C, with gentle stirring, into 30 mM Tris, pH 8.5, containing 1 M ammonium sulfate. The dialyzed protein was bound to a 25-ml Fast-Flow phenyl-Sepharose column (Amersham Biosciences) pre-equilibrated with 1 M ammonium sulfate in 30 mM Tris, pH 8.5, and subsequently eluted with a decreasing gradient of 1 to 0 M ammonium sulfate. The cytochrome was judged pure by SDS-PAGE, concentrated as before, and stored at 4 °C for short term use, or −80 °C for longer term storage. All chromatography procedures were carried out using an AKTAPrime (Amersham Biosciences) purification system, except for the Mono Q column, which was run on an AKTABasic column (Amersham Biosciences). The soluble fraction from a 2-liter culture was also prepared as described above. This soluble fraction was concentrated using a 15-ml 5-kDa molecular weight cut-off centrifugal concentrator (Millipore) to a final volume of 5 ml, and then loaded onto a Superdex 200 16/60 gel-filtration column pre-equilibrated with 20 mM Tris, pH 8.0. Proteins were eluted in the same buffer. Fractions were monitored for presence of protein using the absorbance at 280 nm for the presence of cytochrome using the absorbance at 410 nm. Fractions containing the 6-kDa cytochrome were identified by SDS-PAGE, pooled, and concentrated in a 5-ml 5-kDa MWCO concentrator.

Electronic Absorption Spectroscopy—UV-visible spectra of protein samples were recorded on a Varian Cary 4E UV-visible spectrophotometer between 350 and 650 nm. Reduced samples were achieved by adding excess sodium dithionite and oxidized samples by the addition of potassium ferricyanide.

Electron Transfer Assay—To determine whether purified cytochromes were able to donate electrons to SerABC *in vitro*, a solution of ~5 μM cytochrome in 50 mM phosphate buffer (pH 7.5) was degassed in a sealed cuvette. A weak solution (10 mM) of sodium dithionite was also degassed and then titrated into the cuvette using a 10-μl Hamilton syringe, until the cytochrome was fully reduced, as determined by wavelength scanning UV-visible spectroscopy (350–700 nm). SerABC and selenate were added to final concentrations of 1 μM and 20 mM, respectively, and re-oxidation of the cytochrome was monitored by recording the spectra. Cytochromes were similarly tested for selenate and selenite reductase activity by incubation with the relevant substrate but no SerABC.

Optical Redox Titrations—Optical spectra of the samples were measured on a Hitachi U-3310 spectrophotometer between 350 and 700 nm. Protein samples were added to a stirred cuvette constantly sparged with oxygen-free nitrogen to minimize oxidation from air. Redox mediators (2,3,5,6-tetramethyl-*p*-phenylendiamine, 1,2-napthoquinone, phenozine-methosulfate, phenylethosulfate, juglone, duroquinone, and menadion) were added to a final concentration of 6 μM each, and the potential was measured using an electrode (23). The electrode was initially calibrated with reference to a saturated solution of quinhydrone (295 mV *versus* standard hydrogen electrode). A degassed solution of 5 mM sodium dithionite was prepared and added in 1-μl steps, recording the potential, and the spectra at each step. Once the sample was fully reduced, 3 mM potassium ferricyanide was titrated in similarly to re-oxidize the sample. The fraction of protein reduced at each potential was calculated and fitted to a Nernstian equation using the curve-fitting program TableCurve 2D (Systat Software Inc.).

Sequence Analysis of the 24-kDa Cytochrome—N-terminal sequencing of the 24-kDa cytochrome was undertaken at the Pinnacle Proteomic facility, Newcastle University. Native 24-kDa cytochrome *c* was also digested in solution using Trypsin Gold (Promega, Madison, WI) according to the manufacturer's instructions. Briefly, Trypsin Gold in 50 mM acetic acid was mixed with the cytochrome (in 30 mM Tris, pH 8.5) in a ratio of 1:20 w/w protease:protein. The mixture was incubated at 37 °C for 1 h and analyzed by SDS-PAGE. Protein bands of interest were excised for analysis, which was carried out using liquid chromatography/tandem mass spectrometry at the University of York Proteomics Department.

Sequencing the T. selenatis Genome Using Illumina Sequencing—Genomic DNA was extracted and fragmented to using the Bioruptor apparatus, and fragments of 200 bp were selected using an agarose gel-purification protocol. These fragments were then prepared using the standard Illumina paired-end library-preparation protocols. The resulting DNA was purified using an acrylamide gel, and these were sequenced using an Illumina GA2 sequencer using a single lane loaded at 6 pM. Illumina version 2 reagents were used together with Illumina SCS 2.3 and Illumina Pipeline 1.3 software to base call. This produced 15,422,089 36-bp paired-end sequences. These were subsequently trimmed to remove or shorten reads that contained adaptor sequence. Read 2 contained unusually high error rates toward the 3′-end of the reads. Where appropriate these were shortened prior to any *de novo* assembly to remove bases with quality scores of <20.

MAQ (available on-line from sourceforge.net) was used to align these sequences to the reference genome Thauera MZ1T (GenBank™ accession CP001281 and CP001282). This was achieved with an average depth of 32.9 across non-gap regions.

Unmapped reads were then collated and assembled *de novo* using Velvet (version 0.7.47) in single-end mode using a hash length of 21 (24). These unmapped reads generated an assembly with 14,870 contigs and an N50 length of 1223 bp. These contigs represent genomic regions present in *T. selenatis* but which are absent in Thauera MZ1T. Additionally a completely *de novo* assembly was produced using Velvet in paired-end mode using a parameter sweep of hash length and coverage cut-off. A hash length of 25 and a coverage cut-off of 5 were found to produce the highest N50. This resulted in an assembly of 769 contigs with an N50 value of 135,919 bp (made up of 17 contigs) and a total length of 9.48 Mb.

Micro-culture Growth and Respiratory Inhibition Studies—To monitor the effects of changing culture conditions and inhibitors on the growth of *T. selenatis*, a method utilizing micro-culture was developed. A 500-ml bottle of mineral salts medium was prepared without the addition of selenate or other electron acceptor. The bottle was sealed with rubber septa and sparged with oxygen-free nitrogen for at least 1 h. Each well of a 96-well microtiter plate had 250 μl of the degassed medium added to it, and electron acceptor was added in varying concentrations from degassed stock solutions. Inhibitors, myxothiazol, antimycin A, and 2-*n*-heptyl-4-hydroxyquinoline *N*-oxide (HQNO), at a range of concentrations, were added to wells as required. Wells were inoculated with 1 μl of washed cells from an exponential phase *T. selenatis* culture (1 ml of cells at $A_{600\ nm}$ 0.6–0.7 were harvested by centrifugation at 12,000 $\times$ *g*, 2 min, and resuspended in 1 ml of the degassed medium). Inoculated plates were incubated in a FLUOstar Optima microplate reader (BMG Labtech) attached to a nitrogen cylinder to keep the plate in an anaerobic atmosphere. The plate was maintained at a constant temperature of 30 °C, and $A_{600\ nm}$ values were measured in each well every 15 min using the kinetics-measuring program, with 5-s shaking before each reading. Each plate had 6 wells without the addition of bacteria to ensure no contaminants were growing, and to act as a baseline, and 6 wells with non-inhibiting growing conditions for *T. selenatis* to check the culture was growing typically. The maximum gradient at exponential growth was determined by fitting the growth curves to the Gompertz equation (25). All growth conditions were replicated at a range of substrate concentrations and using non-linear regression; the maximum growth rate (μ_{max}) of the culture was calculated using the Monod equation (Equation 1) (26).

$$\mu = \mu_{max}([S]/K_s + [S]) \qquad \text{(Eq. 1)}$$

RESULTS

Cytochrome c Profile during Selenate Respiration—The *c*-type cytochromes expressed during selenate respiration in *T. selenatis* were profiled by heme staining SDS-PAGE resolved periplasmic proteins. Several soluble cytochromes were identified (referred to as cyt*c*-Ts1–Ts7, in size order) (Fig. 2*A*) and by comparing the expression profile to nitrate grown cells, a number of cytochromes were found to be more highly expressed during selenate respiration. cyt*c*-Ts1 was present under both growth conditions but to a lesser extent when grown on selenate. cyt*c*-Ts2 was poorly resolved but present as a band at ~40 kDa in selenate-grown cells. cyt*c*-Ts3 (~33 kDa) was again expressed under both growth conditions. Cytochromes identified as cyt*c*-Ts5 and cyt*c*-Ts6 were resolved only in selenate grown cells. cyt*c*-Ts4 (24 kDa) and cyt*c*-Ts7 (6 kDa) were both significantly up-regulated under selenate growth conditions and selected for further investigation. cyt*c*-Ts4 and cyt*c*-Ts7 were purified (Fig. 2*A*) and tested as potential electron donors to SerABC.

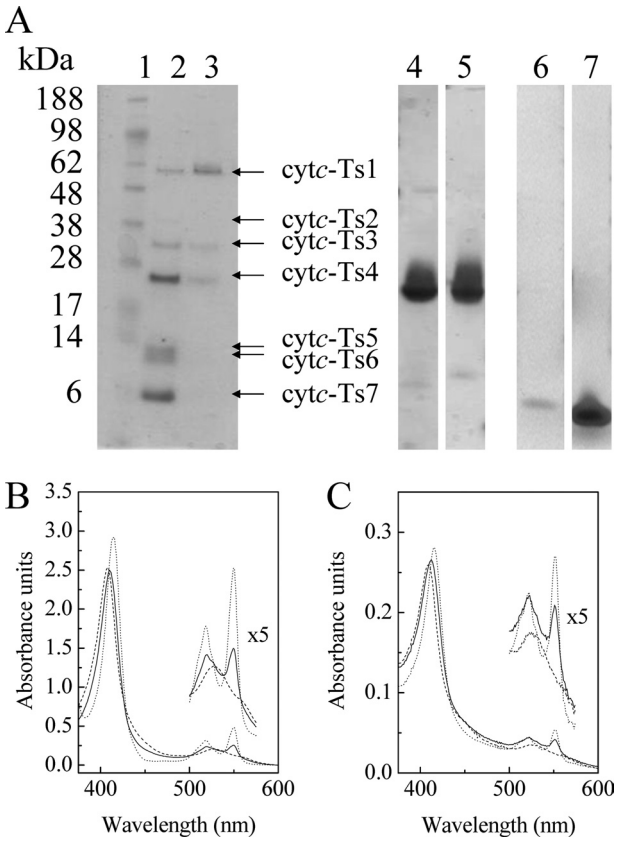

FIGURE 2. **Cytochrome *c* profile from *T. selenatis*.** *A*, SDS-PAGE gels stained for *c*-type cytochromes, showing periplasmic cytochromes (cyt*c*-Ts1–7) expressed during selenate and/or nitrate respiration. *Lane 1*, Invitrogen See-Blue Plus2 Prestained Standard; *lane 2*, periplasmic fraction from selenate grown cells (heme stained); and *lane 3*, periplasmic fraction from nitrate grown cells (heme stained). 7 μg of protein was loaded in each lane. *Lane 4*, purified cyt*c*-Ts4 (~24 kDa) stained with Invitrogen SeeBlue Plus2; *lane 5*, purified cyt*c*-Ts4 (~24 kDa) stained with heme stain; *lane 6*, purified cyt*c*-Ts7 (~6 kDa) stained with Invitrogen SeeBlue Plus2; and *lane 7*, purified cyt*c*-Ts7 (~6 kDa) stained with heme stain. *B*, spectra of 25 μM cyt*c*-Ts4 (~24-kDa protein) as purified (*solid line*), reduced with sodium dithionite (*dotted line*), and oxidized with potassium ferricyanide (*dashed line*). *C*, spectra of 25 μM cyt*c*-Ts7 (~6-kDa protein) as purified (*solid line*), reduced with sodium dithionite (*dotted line*), and oxidized with potassium ferricyanide (*dashed line*).

Characterization of 6-kDa Cytochrome (cytc-Ts7)—The reduced UV-visible spectrum of the purified 6-kDa cytochrome (cyt*c*-Ts7) was typical of a low spin *c*-type cytochrome, with absorbance maxima at 415, 522, and 551 nm (Fig. 2*C*). The oxidized spectrum shows a shift in the Soret band to 409 nm and a broad feature around 525 nm. To test the ability of this cytochrome to donate electrons to SerABC, it was reduced by titration with a weak solution of sodium dithionite, and mixed with purified selenate reductase and selenate in an anaerobic assay. No re-oxidation of the heme was observed suggesting that the 6-kDa cytochrome is not able to act as an electron donor to SerABC *in vitro* (data not shown).

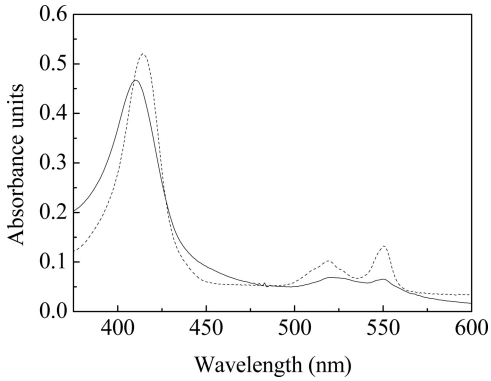

FIGURE 3. **Spectroscopic assay of electron donation from cytc-Ts4 to SerABC.** cytc-Ts4 (5 μM) reduced with dithionite (*dashed line*) was mixed with 1 μM SerABC and 20 mM selenate and re-oxidation was monitored by wavelength scanning UV-visible spectroscopy (*solid line*).

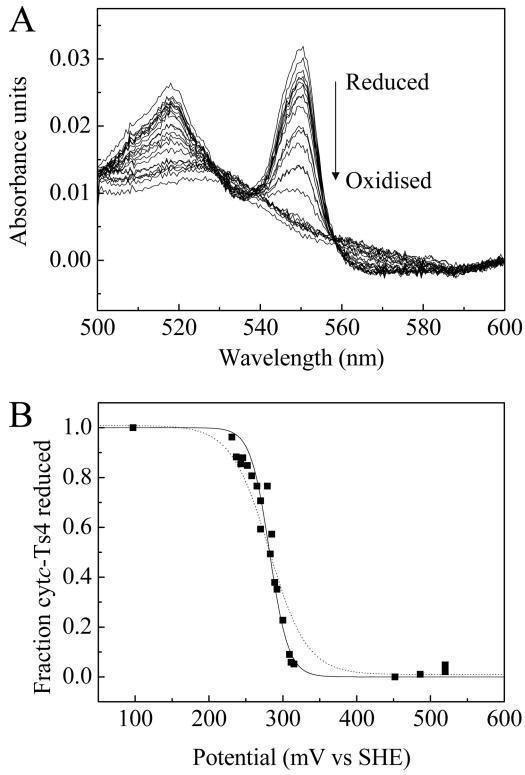

FIGURE 4. **Optical redox titration of cytc-Ts4.** *A*, α and β region of cytc-Ts4 spectrum during titrations. The *black arrow* indicates increasing redox potential. *B*, fraction of cytochrome reduced as calculated with reference to absorbance at 551 nm, as a function of redox potential. Nernst curves for $n = 1$ electrons (*dashed line*) and $n = 2$ electrons (*solid line*) are also shown.

Characterization of the 24-kDa Cytochrome (cytc-Ts4)—UV-visible spectroscopy of the 24-kDa cytochrome (cytc-Ts4) was again typical of a low spin heme *c* (Fig. 2*B*). It was purified in a partially reduced state, but did not readily become oxidized, even after lengthy exposure to air. Protein reduced with dithionite showed a Soret band at 414 nm, an α-band at 550 nm, and a β-band at 519 nm. The α-band showed asymmetry, with a shoulder at 545 nm suggesting a composite band, possibly due to the presence of more than one heme in the protein. Oxidized with ferricyanide, the cytochrome had a Soret band at 409 nm and a broad feature at 528 nm. As for cytc-Ts7, cytc-Ts4 was tested for its ability to donate electrons to SerABC in an anaerobic assay. In this case, after incubation with enzyme and substrate, the visible absorbance spectrum was shifted (Fig. 3). The Soret band shifted from 414 to 410 nm, and decreased in intensity, and the α/β peaks broadened and decreased in intensity, indicative of re-oxidation of the heme. cytc-Ts4 incubated with SerABC, selenate, or selenite alone did not exhibit any shifts in absorbance (data not shown), suggesting that this cytochrome is capable of donating electrons to SerABC for the reduction of selenate to selenite *in vitro*, and therefore could be an *in vivo* electron donor to SerABC. The rate of cytc-Ts4 heme oxidation was determined to be some 50 times slower than the observed rate of SER turnover determined using methyl viologen as the electron donor (6). Similarly, Craske and Ferguson (27) have shown that NAR from *Paracoccus denitrificans* has a 50-fold higher V_{max} with methyl viologen than with duroquinol.

Determination of the Redox Potential of cytc-Ts4—The redox potential of the heme of cytc-Ts4 was measured spectrophotometrically by monitoring the absorbance of the α-band at 551 nm (adjusted by reference to an isosbestic point at 560 nm) during reduction or oxidation of the heme (Fig. 4*A*). The fraction of protein reduced at each measured potential was calculated, then plotted as a function of redox potential *versus* the standard hydrogen electrode (Fig. 4*B*). Nernst curves for $n = 1$ and $n = 2$ (where n is the number of electrons transferred) were fitted and are also shown in Fig. 4*B*. Interestingly, the data fits more closely to an $n = 2$ curve, suggesting the cytochrome has two hemes. A mid-point potential of +282 ± 10 mV for the cytochrome was calculated, but we were unable to resolve two separate potentials.

Sequence Determination and Analysis—MALDI-TOF analysis of cytc-Ts4 gave a molecular mass of 23,558 Da, not including heme groups. N-terminal sequencing (Pinnacle Proteomic facility, Newcastle University) and liquid chromatography/tandem mass spectrometry of tryptic digest fragments (University of York Proteomics Department) resulted in 60 amino acids of sequence data, which was used to identify the gene for this cytochrome from the draft genome assembly of *T. selenatis*. Peptides were searched against a custom Blast (28) database containing all contigs generated from the sequence data, which could not be mapped to Thauera MZ1T and separately to another database containing the complete set of contigs generated from all Illumina *T. selenatis* data. Due to the short lengths of the peptides only two significant hits were obtained, and these contigs were used as targets for further investigation. Open reading frame prediction was carried out using the CLC-Bio software package, and candidate regions were searched via Blast against the non-redundant database of protein sequences. The sequence of cytc-Ts4 (GenBank™ accession GU570563) was used to search the database, and an alignment of similar cytochromes is shown in supplemental Fig. S1. Alignment of the predicted amino acid sequences shows the presence of two conserved C*XX*CH motifs consistent with the binding of two covalently attached hemes. The presence of two further conserved methionine residues suggests that both hemes are His-Met coordinated.

Determination of the Redox Potential of the b-heme in SerC—Purified SER was used to determine the midpoint potential of

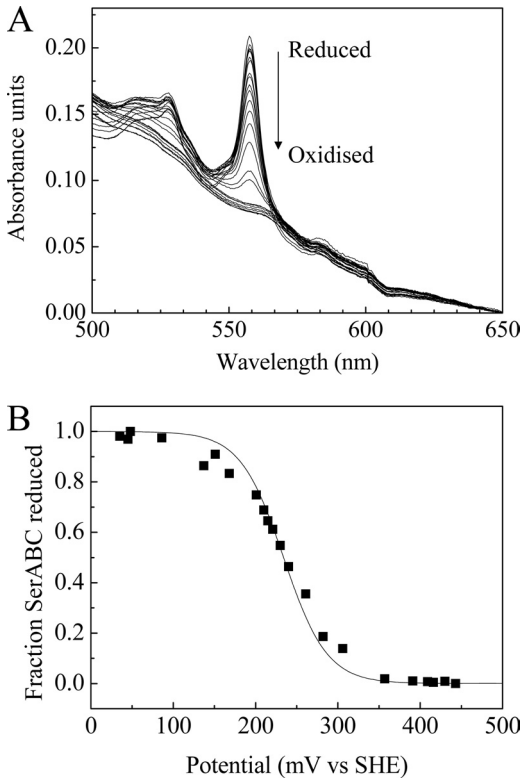

FIGURE 5. **Optical redox titration of SerC.** *A*, the α and β region of *b*-heme spectrum during titrations. The *black arrow* indicates increasing redox potential. Samples were prepared in 30 mM Tris-HCl, pH 7.5. *B*, fraction of cytochrome *b* reduced as calculated with reference to absorbance at 558 nm, as a function of redox potential. Nernst curve for $n = 1$ electron.

the *b*-heme in SerC, the point of electron entry to the reductase from the cyt*c* redox partner. The redox potential of the heme was determined by optical redox titration by monitoring the absorbance of the heme at 558 nm (adjusted with reference to an isosbestic point at 575 nm) during sequential oxidation and reduction of the heme (Fig. 5*A*). The slight drift observed in the spectrum was due to the contribution of the [Fe-S] clusters in SerAB. The absorbance was monitored at the α-band wavelength rather than that of the Soret band, because the redox mediators used do not absorb in the α-band region, but might interfere at Soret band wavelengths. The fraction of protein reduced at each measured potential was calculated and then plotted as a function of redox potential (Fig. 5*B*). The Nernst curve corresponding to $n = 1$ electrons was fitted to the data giving a midpoint potential of $+234 \pm 10$ mV.

Quinol-cytochrome c Oxidoreductase Is an Electron Donor to Selenate Reductase in T. selenatis—Soluble cytochromes acting as electron carriers need to accept electrons from an upstream donor. Commonly, this comes in the form of a QCR, which can contribute to the PMF via the Q-cycle. To investigate whether the QCR is involved in selenate respiration and could therefore be responsible for electron transfer to the di-heme cytochrome (cyt*c*-Ts4), classic inhibitors of respiratory chains were used during selenate and nitrite respiration. The inhibitors myxothiazol and antimycin A specifically inhibit the QCR, but at different sites (29). Myxothiazol binds to the Q_o site on the *b* heme subunit of QCR. The Q_o site is where quinol is oxidized to quinone, and the binding of myxothiazol stops electrons being transferred from the Q-pool to downstream electron acceptors. By contrast, antimycin A binds to the Q_i site of QCR preventing the reduction of quinone to quinol. HQNO is a less specific quinone analogue, which inhibits not only the QCR (30), but also the membrane-bound nitrate reductase subunit NarI (31) and multi-heme quinol dehydrogenases such as NrfH from *Wolinella succinogenes* nitrite reductase (32).

To culture *T. selenatis* under more reproducible conditions, and allow multiple replicates of growth curves, a method of culturing *T. selenatis* in a 96-well microplate was devised. All growth conditions were replicated in 10 wells, allowing averaging of the optical densities over each time point. Before averaging, the optical density of a control set of wells of medium with no bacterial culture was subtracted from the growth curves. To test whether concentrations of inhibitor were high enough to inhibit *T. selenatis*, the microplate method was used to investigate the effect of myxothiazol on nitrite respiration, to see if complete inhibition could be achieved. *Thauera* sp. is known to express a cd_1 nitrite reductase (33, 34), which commonly receives its electrons from the QCR via soluble intermediates (35). A range of nitrite concentrations was used, with myxothiazol at 10 μM. Ten wells contained 5 mM nitrite, but no inhibitor. Myxothiazol was seen to inhibit nitrite respiration very effectively, and no growth was observed (Fig. 6*A*). This confirms the effectiveness of myxothiazol as an inhibitor of the QCR in *T. selenatis*.

T. selenatis was cultured under selenate respiratory conditions, with varying concentrations of selenate and 10 μM myxothiazol. Ten wells contained 10 mM selenate but lacked myxothiazol, as a positive control. The resulting growth curves (Fig. 6*A*) indicate that selenate respiration is partially inhibited by myxothiazol, suggesting that the QCR is involved in this process. The experiments were repeated in the presence of the inhibitor antimycin A (at both 10 and 20 μM), and the results (Fig. 6*B*) are consistent with the observations made using myxothiazol, strongly indicating the involvement of QCR in electron transport. Again, even at 20 μM antimycin, some growth is detected (final $A_{600\,nm} \sim 0.3$ unit). Analysis of the specific growth rates (μ_{max}) at increasing selenate concentration shows that K_s is unaffected (~2.5 mM); however, in the presence of myxothiazol, a 3-fold decrease in μ_{max} is recorded (no inhibitor $= 0.32 \pm 0.03\ h^{-1}$; plus myxothiazol $= 0.10 \pm 0.02\ h^{-1}$) (Fig. 6*C*). Therefore, it can be seen, from the growth curve analysis, that both myxothiazol and antimycin A retarded the growth rate of *T. selenatis* during selenate respiration but did not inhibit it completely.

Inhibition of Selenate Respiration by HQNO—Because myxothiazol has been shown to fully inhibit the QCR in nitrite reduction, but is only partially effective at inhibiting selenate respiration, HQNO was used as an inhibitor that affects a wider range of proteins with quinol dehydrogenase activity. HQNO was shown to inhibit growth completely with no significant change in culture *A* for ~14 h post inoculation. Cultures maintained for 14–18 h showed a slight increase in culture *A* presumably due to the breakdown or evaporation of HQNO from the growth medium (Fig. 6*A*). By combining both inhibitors, HQNO and myxothiazol, there was no significant difference between the growth curves obtained with HQNO alone. The

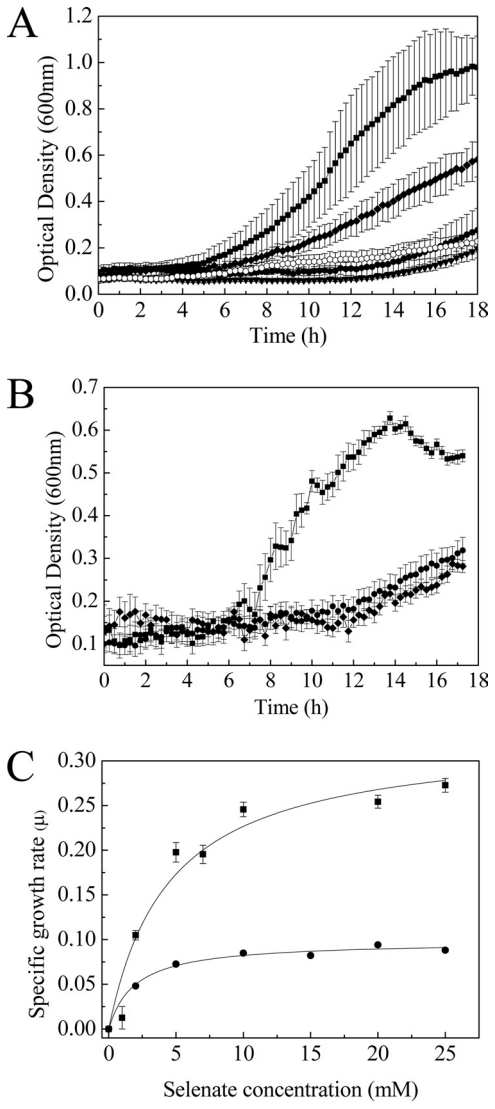

FIGURE 6. **Inhibition of respiration by myxothiazol, antimycin A, and HQNO.** *A*, optical density of *T. selenatis* cultures grown with 10 mM selenate as electron acceptor in the absence and presence of inhibitors. Shown are no inhibitor (■), 10 μM myxothiazol (◆), 20 μM HQNO (●), and both 10 μM myxothiazol and 20 μM HQNO (▼). Positive control: *T. selenatis* grown with 5 mM nitrite as electron acceptor in the presence of 10 μM myxothiazol (○). *B*, optical density of *T. selenatis* cultures grown with 10 mM selenate as electron acceptor in the absence and presence of antimycin A. Shown are no inhibitor (■), 10 μM antimycin A (◆), and 20 μM antimycin A (●). *C*, specific growth rate (μ_{max}) of *T. selenatis* cultures grown on increasing selenate concentration in the absence (■) and presence (●) of myxothiazol (10 μM). In all cases *error bars* represent standard deviation of $n = 10$ cultures.

results (Fig. 6*A*) show that partial inhibition of selenate respiration is obtained by myxothiazol (and antimycin A), whereas complete inhibition of selenate respiration is obtained by HQNO. The combined data suggest that there is more than one route by which electrons can be transferred to selenate reductase: via the QCR, which is inhibited by myxothiazol and antimycin A, and via another type of quinol dehydrogenase, which is inhibited by HQNO.

DISCUSSION

The bioenergetics of selenate respiration in *T. selenatis* has remained unresolved since the isolation of *T. selenatis* by Macy and co-workers in 1993 (36). The respiration of selenate results in the sequential reduction of selenate to selenite to elemental selenium, yet it is only selenate that can function as a respiratory substrate. SER is a soluble molybdoenzyme composed of three subunits and is expressed from an operon of four genes (7), three for the structural components and the forth (SerD) a private chaperone for the functional assembly of SerA. No obvious membrane-bound component has been identified. Although others have speculated as to how SER receives electrons from the Q-pool and how this is coupled to the generation of PMF (21), biochemical evidence for the electron transfer pathway in *T. selenatis* has remained wanting. In the present study we have demonstrated that SER can receive electrons from a di-heme cytochrome of the cytc_4 family and is driven by electron transfer via a branched pathway that includes electron transfer from QCR or QDH. The demonstration of an electron transfer pathway to a periplasmic molybdoezyme that utilizes a high potential di-heme cytochrome *c* carrier and electron flux through QCR is the first of its kind and unprecedented in other molybdo-oxidoreductase systems.

A number of periplasmic *c*-type cytochromes were up-regulated when *T. selenatis* was grown on selenate as the sole electron acceptor. During this study, two of these cytochromes have been purified and tested as potential redox partners to SER. A 24-kDa cytochrome, termed cyt*c*-Ts4, was shown to donate electrons to SER and was characterized further. N-terminal sequence and liquid chromatography/tandem mass spectrometry analyses identified peptides as those resulting from members of the cytochrome c_4 family. Attempts to use PCR and sequence the cyt*c*-Ts4 gene using degenerate primers derived from other c_4 homologues failed. Consequently, a holistic approach was adopted, and the entire genome of *T. selenatis* was sequenced using an Illumina sequencer. The complete cyt*c*-Ts4 gene sequence was subsequently identified. A database search with the translated sequence of this gene produced a large number of similar proteins, most of which are classified as cytochromes c_4, a group of di-heme cytochromes *c* characterized by high redox potentials, a low intensity asymmetrical α band around 550 nm and a low α/β peak ratio (37, 38). A number of members of this group have been characterized, including members from *Acidithiobacillus ferrooxidans* (39, 40), *Pseudomonas stutzeri* (41), *Thiocapsa roseopersicina* (42), and *Azotobacter vinelandii* (43). Cytochromes c_4 have been proposed to be electron donors to oxidases due to the presence of a cytochrome c_4 in the aerobe *A. vinelandii* (43), but the discovery of a cytochrome c_4 in *T. roseopersicina*, a facultative anaerobic photosynthetic bacterium, suggests that their roles are much more varied (42, 44). Recently, a cytc_4 has also been found to function as a physiological electron carrier in the photosynthetic electron transport chain in *Rubrivivax gelatinosus* (45).

Structural data are available for two cytochromes c_4, from *P. stutzeri* (46) and *A. ferrooxidans* (47). The two hemes in each case both have His-Met axial ligation, and the methionine residues identified as ligands are conserved throughout the cytochrome c_4 group, and in the cyt*c*-Ts4. The sequence similarity and high redox potential of the 24-kDa cytochrome suggest that we can assign cyt*c*-Ts4 to the cytochrome c_4 group. The involvement of a c_4 cytochrome in anaerobic selenate respiration defines a new role for this class of cytochromes.

Of the other cytochromes up-regulated during growth of *T. selenatis* on selenate, a 6-kDa cytochrome was also purified (cyt*c*-Ts7). No evidence was obtained to suggest that cyt*c*-Ts7 could transfer electrons to SER. Furthermore, no direct reduction of selenate or selenite was observed. The function of cyt*c*-Ts7 remains to be established. Chlorate reductase from *I. dechloratans* is also a member of the TAT-translocated type II molybdoenzymes and is closely related to SER. It has been shown recently that a 6-kDa cytochrome from *I. dechloratans* was readily oxidized in the presence of chlorate and cell homogenate containing chlorate reductase (48), suggesting that a 6-kDa cytochrome could be the redox partner for chlorate reductase. The authors suggest that the 6-kDa cytochrome might accept electrons from QCR, but no biochemical evidence for the involvement of QCR was reported. More recently, a cytochrome *c* gene located at the gene cluster for chlorate respiration in *I. dechloratans* has been cloned and overexpressed in *E. coli* but demonstrated not to function as an electron donor to purified chlorate reductase (49). It is interesting to speculate what the functions of the additional *c*-type cytochromes are in *T. selenatis* when grown on selenate. The mechanism by which selenite is reduced remains unknown. What is clear is that the reduction of selenite results in the formation of selenium nanospheres that are found in the surrounding medium. For the elemental selenium to form extracellular particles, it is considered likely that selenite is reduced either in the periplasm or on the outer cell surface, and as a consequence the other cytochromes identified might form an electron conduit to selenite reductase.

The involvement of QCR in the respiratory electron transfer chain of *T. selenatis* was suggested from the genome analysis (GenBank™ accession EU732596.1) and confirmed by complete inhibition of nitrite respiration by myxothiazol. *T. selenatis* expresses a cd_1 nitrite reductase (also identified in the *T. selenatis* genome (GenBank™ accession AY078264.1), which commonly receives electrons from QCR via soluble intermediates (cytochromes/azurins). Selenate respiration was only partially inhibited (70% reduction in μ_{max}) by the same concentration of myxothiazol or antimycin A and completely inhibited by HQNO. QCR binds two quinol molecules at the periplasmic face of the membrane and moves two electrons to the cytoplasmic face of the membrane, where it reduces one quinone molecule. This so-called Q-cycle translocates two positive charges per quinol oxidized. Given that myxothiazol and antimycin A are specific inhibitors of QCR, a redox loop coupling a Q-cycle mechanism to selenate reduction would seem plausible. HQNO is a less specific quinone analogue, which inhibits both QCR and other membrane-bound QDHs (31, 32). HQNO alone, or in combination with myxothiazol, resulted in the complete inhibition of growth of *T. selenatis*. These data suggest that selenate reductase can accept electrons from more that one electron donor. A branched pathway that involves both QCR and QDH is proposed (Fig. 7). A QDH partner has not been identified, but analysis of the *c*-type cytochromes in membrane fractions from *T. selenatis*, grown on selenate, reveals that cytochromes of ~30 and ~20 kDa are present, but attempts to purify these components have so far proved unsuccessful (data not shown). A *nap*C/*nir*T homologue (50) has also been identified in the *T. selenatis* genome that could be a likely candidate.

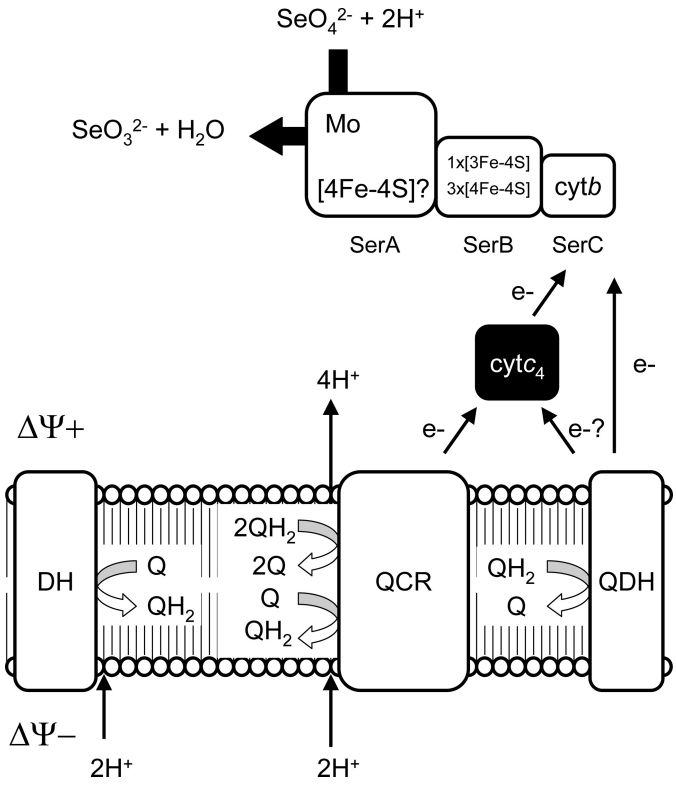

FIGURE 7. **Schematic diagram showing the electron transport chain of *T. selenatis* during anaerobic growth on selenate.**

The ability to utilize a QCR-dependent bioenergetic pathway is facilitated by the high redox potential of the selenate/selenite couple (E_m +475 mV). This allows the selenate reductase to function by using a high potential cytochrome *c* as the electron donor. The interesting feature of SER thus relates to the point of electron entry and the unusual *b*-heme in SerC. The determination of the redox potential of the SerC heme has allowed us to add to our knowledge of the redox centers of the selenate reductase and is the first periplasmic reductase of the Type II molybdoenzymes to have the potential of its *b*-heme determined. Supplemental Fig. S2 shows the known midpoint potentials of all redox centers within SER, from the redox potential of the substrate to the potential of *b*-heme subunit. The value of E_m = +234 ± 10 mV for the SerC *b*-heme is very similar to that determined for EbdC (+254 mV). EBDH functions by withdrawing electrons from ethylbenzene, where the *b*-heme functions as an electron attractant. Conceptually, to convert from a dehydrogenase function to a reductase function, one might assume that the potential of the corresponding *b*-heme in the type II molybdoreductases might be retuned to function at a much lower redox-potential, thus facilitating electron donation. This appears not to be the case for selenate reductase. It is of interest to compare SerC/EbdC cytochromes to the membrane-bound cytochrome associated with the respiratory nitrate reductase (NarI). NarI contains two *b*-hemes, but both have much lower redox potential (+120 and +20 mV). Modeling the three-dimensional structure of SerC, using the x-ray coordinates of EbdC from *A. aromaticum*, predicts that the

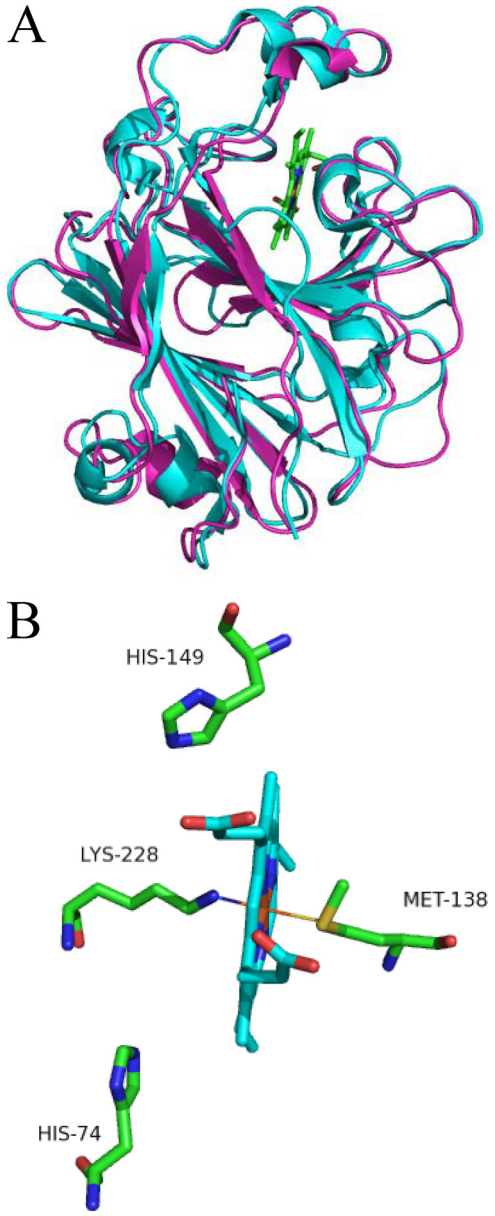

FIGURE 8. ***b*-Heme coordination in SerC.** *A*, predicted structure of SerC modeled upon the crystal structure of EBDH γ-subunit. The superposition shows SerC in *green* and the EbdC in *cyan*. *B*, detail of heme pocket showing ligands. Homology modeling was performed using the homology tools in the software package MOE™. The sequence of *T. selenatis* SerC was aligned and modeled against the structure of EBDH γ-subunit from *A. aromaticum* (PDB ID 2IVF C). The sequence was modeled from residues 27–239. The modeling was performed using the protein template alone, and additionally using the environment of the template structure with the heme ligand. An ensemble of 30 intermediate models was created, and the best intermediate model as minimized using the CHARM22 force field to a root mean square gradient of 0.01. The quality of the models was assessed by PROCHECK (52, 53). Analysis of the model structure and generation of molecular images were carried out using PyMOL (54).

b-heme in SerC is also coordinated by methionine (Met-138) and lysine (Lys-228) ligands (Fig. 8). In NarI, both hemes have iron with *bis*-histidinyl coordination, and this could contribute to the differences in redox potential. The sulfur of methionine residues is a good electron acceptor and could contribute to stabilizing the reduced state of the heme, therefore significantly raising the midpoint potential.

Evidently the combination of a high potential *b*-heme in SerC and the unusual high potential redox couple of the substrate (selenate/selenite) has provided a system that can readily accept electrons from cyt-*c* and QCR redox partners. By using these redox partners, selenate reduction can be linked to a Q-cycle mechanism. Because selenate reductase functions on the positive side of the cytoplasmic membrane, the reduction of selenate to selenite will consume two pumped protons. If SER was to receive electrons only from a membrane-bound QDH, then only two protons would be released to the periplasm, resulting in no net gain of proton electro-chemical gradient ($0q^+/2e^-$). Because the reduction of selenite to selenium does not support growth, selenate reduction via a QDH could only be energy conserving if electron input into the Q-pool was proton-motive (*i.e.* via an NADH dehydrogenase, a formate dehydrogenase, or hydrogenase). By using the Q-cycle mechanism a net gain of $2q^+/2e^-$ of proton electrochemical gradient can be maintained irrespective of the electron donor.

Finally, the Q-cycle-coupling mechanism presented for selenate reduction in *T. selenatis*, while a novel mechanism for electron transport to molybdoenzymes in bacteria, might also be utilized in the Archaea (51). Sequence analysis has suggested that the clade of TAT-translocated type II molybdoenzymes, of which SER is a member, also contains a number of unusual respiratory nitrate reductases (pNAR). These reductases all possess a TAT leader peptide and are translocated to the positive side of the membrane. The pNAR enzymes are distributed among the Archaea, and examples have been identified in the hyperthermophiles and halophiles. Interestingly, those from halophiles (*Haloferax mediterranei* and *Haloarcula marismortui*) lack a NarI-like component so the mechanism of electron transport is not obvious. However, genetic analysis reveals the presence of a sequence that encodes a protein (NarC) similar to the di-heme subunits of QCR. Adjacent to the *nar*C gene is a gene that encodes NarB, which is predicted to encode a Rieske iron-sulfur protein. The combination of NarB and NarC in *H. mediterranei* has led to the suggestion that nitrate respiration in some organisms might be driven by a Q-cycle mechanism (51). By coupling a Q-cycle mechanism to nitrate reduction would provide a pNAR system that is bioenergetically equivalent to the well characterized NAR (or nNAR) systems in bacteria.

Acknowledgments—We thank Ann Reilly (University of East Anglia), Iona Knight (University of Exeter), and Dr. Carys Watts and Dr. Helen Ridley (University of Newcastle) for technical support and useful discussions. We also thank Dr. Kirsty Line (University of Exeter) for providing structural models.

REFERENCES

1. McDevitt, C. A., Hugenholtz, P., Hanson, G. R., and McEwan, A. G. (2002) *Mol. Microbiol.* **44,** 1575–1587
2. Berks, B. C., Sargent, F., and Palmer, T. (2000) *Mol. Microbiol.* **35,** 260–274
3. Sargent, F. (2007) *Microbiology SGM* **153,** 633–651
4. Johnson, H. A., Pelletier, D. A., and Spormann, A. M. (2001) *J. Bacteriol.* **183,** 4536–4542
5. McDevitt, C. A., Hanson, G. R., Noble, C. J., Cheesman, M. R., and McEwan, A. G. (2002) *Biochemistry* **41,** 15234–15244
6. Schröder, I., Rech, S., Krafft, T., and Macy, J. M. (1997) *J. Biol. Chem.* **272,**

23765–23768
7. Krafft, T., Bowen, A., Theis, F., and Macy, J. M. (2000) *DNA Seq.* **10,** 365–377
8. Thorell, H. D., Stenklo, K., Karlsson, J., and Nilsson, T. (2003) *Appl. Environ. Microbiol.* **69,** 5585–5592
9. Karlsson, J., and Nilsson, T. (2005) *Protein Expr. Purif.* **41,** 306–312
10. Creevey, N. L., McEwan, A. G., Hanson, G. R., and Bernhardt, P. V. (2008) *Biochemistry* **47,** 3770–3776
11. Dridge, E. J., Watts, C. A., Jepson, B. J., Line, K., Santini, J. M., Richardson, D. J., and Butler, C. S. (2007) *Biochem. J.* **408,** 19–28
12. Richardson, D. J. (2000) *Microbiology* **146,** 551–571
13. Stolz, J. F., Basu, P., Santini, J. M., and Oremland, R. S. (2006) *Annu. Rev. Microbiol.* **60,** 107–130
14. Maher, M. J., Santini, J., Pickering, I. J., Prince, R. C., Macy, J. M., and George, G. N. (2004) *Inorg. Chem.* **43,** 402–404
15. Kloer, D. P., Hagel, C., Heider, J., and Schulz, G. E. (2006) *Structure* **14,** 1377–1388
16. Bertero, M. G., Rothery, R. A., Palak, M., Hou, C., Lim, D., Blasco, F., Weiner, J. H., and Strynadka, N. C. (2003) *Nat. Struct. Biol.* **10,** 681–687
17. McCrindle, S. L., Kappler, U., and McEwan, A. G. (2005) *Adv. Microb. Physiol.* **50,** 147–198
18. Jormakka, M., Richardson, D., Byrne, B., and Iwata, S. (2004) *Structure* **12,** 95–104
19. Potter, L., Angove, H., Richardson, D., and Cole, J. (2001) *Adv. Microb. Physiol.* **45,** 51–112
20. Brondijk, T. H., Nilavongse, A., Filenko, N., Richardson, D. J., and Cole, J. A. (2004) *Biochem. J.* **379,** 47–55
21. McEwan, A. G., Ridge, J. P., McDevitt, C. A., and Hugenholtz, P. (2002) *Geomicrobiol. J.* **19,** 3–21
22. Ridley, H., Watts, C. A., Richardson, D. J., and Butler, C. S. (2006) *Appl. Environ. Micro.* **72,** 5173–5180
23. Dutton, P. L. (1978) in *Methods in Enzymology; Biomembranes E, Specialized Techniques* (Fleischer, S., and Packer, L., eds) Vol. 54, pp. 411–435, Academic Press, New York
24. Zerbino, D. R., and Birney, E. (2008) *Genome Res.* **18,** 821–829
25. Zwietering, M. H., Rombouts, F. M., and van't Riet, K. (1992) *J. Appl. Bacteriol.* **72,** 139–145
26. Monod, J. (1942) *Recherches sur la Croissance des Cultures Bactâeriennes*, p. 211. Hermann, Paris
27. Craske, A., and Ferguson, S. J. (1986) *Eur. J. Biochem.* **158,** 429–436
28. Altschul, S. F., Gish, W., Miller, W., Myers, E. W., and Lipman, D. J. (1990) *J. Mol. Biol.* **215,** 403–410
29. Thierbach, G., and Reichenbach, H. (1981) *Biochim. Biophys. Acta* **638,** 282–289
30. Van Ark, G., and Berden, J. A. (1977) *Biochim. Biophys. Acta* **459,** 119–127
31. Magalon, A., Rothery, R. A., Lemesle-Meunier, D., Frixon, C., Weiner, J. H., and Blasco, F. (1998) *J. Biol. Chem.* **273,** 10851–10856
32. Simon, J. (2002) *FEMS Microbiol. Rev.* **26,** 285–309
33. Etchebehere, C., and Tiedje, J. (2005) *Appl. Environ. Microbiol.* **71,** 5642–5645
34. Song, B., and Ward, B. B. (2003) FEMS. *Microbiol. Ecol.* **43,** 349–357
35. Moir, J. W., Baratta, D., Richardson, D. J., and Ferguson, S. J., (1993) *Eur. J. Biochem.* **212,** 377–385
36. Macy, J. M., Rech, S., Auling, G., Dorsch, M., Stackenbrandt, E., and Sly, L. I. (1993) *Int. J. Syst. Bacteriol.* **43,** 135–142
37. Pettigrew, G. W., and Moore, G. R. (1987) *Cytochromes c: Biological Aspects*, Springer, Berlin
38. Pettigrew, G. W., and Brown, K. R. (1988) *Biochem. J.* **252,** 427–435
39. Cavazza, C., Giudici-Orticoni, M. T., Nitschke, W., Appia, C., Bonnefoy, V., and Bruschi, M. (1996) *Eur. J. Biochem.* **242,** 308–314
40. Giudici-Orticoni, M. T., Leroy, G., Nitschke, W., and Bruschi, M. (2000) *Biochemistry* **39,** 7205–7211
41. Christensen, H. E. (1994) *Gene* **144,** 139–140
42. Branca, R. M., Bodü, G., Várkonyi, Z., Debreczeny, M., Osz, J., and Bagyinka, C. (2007) *Arch. Biochem. Biophys.* **467,** 174–184
43. Swank, R. T., and Burris, R. H. (1969) *Biochim. Biophys. Acta* **180,** 473–489
44. Branca, R. M., Bodü, G., Bagyinka, C., and Prokai, L. (2007) *J. Mass. Spectrom.* **42,** 1569–1582
45. Ohmine, M., Matsuura, K., Shimada, K., Alric, J., Verméglio, A., and Nagashima, K. V. (2009) *Biochemistry* **48,** 9132–9139
46. Kadziola, A., and Larsen, S. (1997) *Structure* **5,** 203–216
47. Abergel, C., Nitschke, W., Malarte, G., Bruschi, M., Claverie, J. M., and Giudici-Orticoni, M. T. (2003) *Structure* **11,** 547–555
48. Bäcklund, A. S., Bohlin, J., Gustavsson, N., and Nilsson, T. (2009) *Appl. Environ. Microbiol.* **75,** 2439–2445
49. Bohlin, J., Bäcklund, A. S., Gustavsson, N., Wahlberg, S., and Nilsson, T. (2009) *Microbiol. Res.*, in press
50. Roldán, M. D., Sears, H. J., Cheesman, M. R., Ferguson, S. J., Thomson, A. J., Berks, B. C., and Richardson, D. J. (1998) *J. Biol. Chem.* **273,** 28785–28790
51. Martinez-Espinosa, R. M., Dridge, E. J., Bonete, M. J., Butt, J. N., Butler, C. S., Sargent, F., and Richardson, D. J. (2007) *FEMS Microbiol. Lett.* **276,** 129–139
52. Morris, A. L., MacArthur, M. W., Hutchinson, E. G., and Thornton, J. M. (1992) *Proteins* **12,** 345–364
53. Laskowski, R. A., MacArthur, M. W., Moss, D. S., and Thornton, J. M. (1993) *J. Appl. Cryst.* **26,** 283–291
54. DeLano, W. L. (2002) The PyMOL Molecular Graphics System, DeLano Scientific, San Carlos, CA

Quinol-cytochrome *c* Oxidoreductase and Cytochrome c_4 Mediate Electron Transfer during Selenate Respiration in *Thauera selenatis*

Elisabeth C. Lowe, Sarah Bydder, Robert S. Hartshorne, Hannah L. U. Tape, Elizabeth J. Dridge, Charles M. Debieux, Konrad Paszkiewicz, Ian Singleton, Richard J. Lewis, Joanne M. Santini, David J. Richardson and Clive S. Butler

J. Biol. Chem. 2010, 285:18433-18442.
doi: 10.1074/jbc.M110.115873 originally published online April 13, 2010
